ORIGINAL PAPER

Influence of Counter-Face Grit Size and Lubricant on the Abrasive Wear Behaviour of Thermoplastic Polymers Reinforced with Glass Fibres

Moustafa Mahmoud Yousry Zaghloul[1,2] · Karen Steel[3] · Martin Veidt[1,2] · Darren Martin[3] · Mahshid Firouzi[4] · Michael T. Heitzmann[1,2]

Abstract

Thermoplastic composite materials are widely used for aerospace, automobile and structural applications due to their good combination of high strength to weight ratio and specific modulus. Combined with the ease of melt processing, good resistance to corrosion, low friction, and noise damping are attributes which make them a popular choice in a wide range of emerging applications. Random, short-fibre, E-glass fibre reinforced Polyamide 6 (PA6) composites were manufactured by injection moulding in three different fibre volume fractions (25%, 33% and 50%) and the samples were scanned using micro-CT. The tribological properties of PA6 and glass fibre reinforced PA6 were investigated in the abrasive wear mode by using a pin-on-disc test setup. The tests were done at an abrading distance of 257 m and applied load of 10 N. The abrasive wear experiments were performed against three abrasive grit size papers (220, 500 and 1000 grit), to ascertain the wear response of the studied materials with respect to these adverse running conditions. Moreover, the mechanical properties of PA6 and PA6 composites were examined using tensile testing and compression testing. The surface roughness of the worn surfaces was analysed using a 3D digital profilometer. The worn surface topographies were scanned using field emission scanning electron microscopy. It was observed that the optimum fibre loading that was associated with the highest wear resistance was 33% volume fraction of glass fibres, and the wear performance deteriorated with higher fibre loadings. The increase in the grit size showed a significant reduction to the wear rates of all compositions. The results confirmed that the wear performance of polyamide composites is highly dependent on the tribological system under which it is being tested.

✉ Moustafa Mahmoud Yousry Zaghloul
Moustafa.Mahmoud@uq.edu.au;
Eng_Moustafaa@hotmail.com

1   School of Mechanical and Mining Engineering, The University of Queensland, Brisbane, Australia

2   Centre for Advanced Materials Processing and Manufacturing (AMPAM), The University of Queensland, Brisbane, Australia

3   School of Chemical Engineering, The University of Queensland, Brisbane, Australia

4   College of Engineering, Science and Environment, The University of Newcastle, Callaghan, NSW 2308, Australia

Graphical Abstract
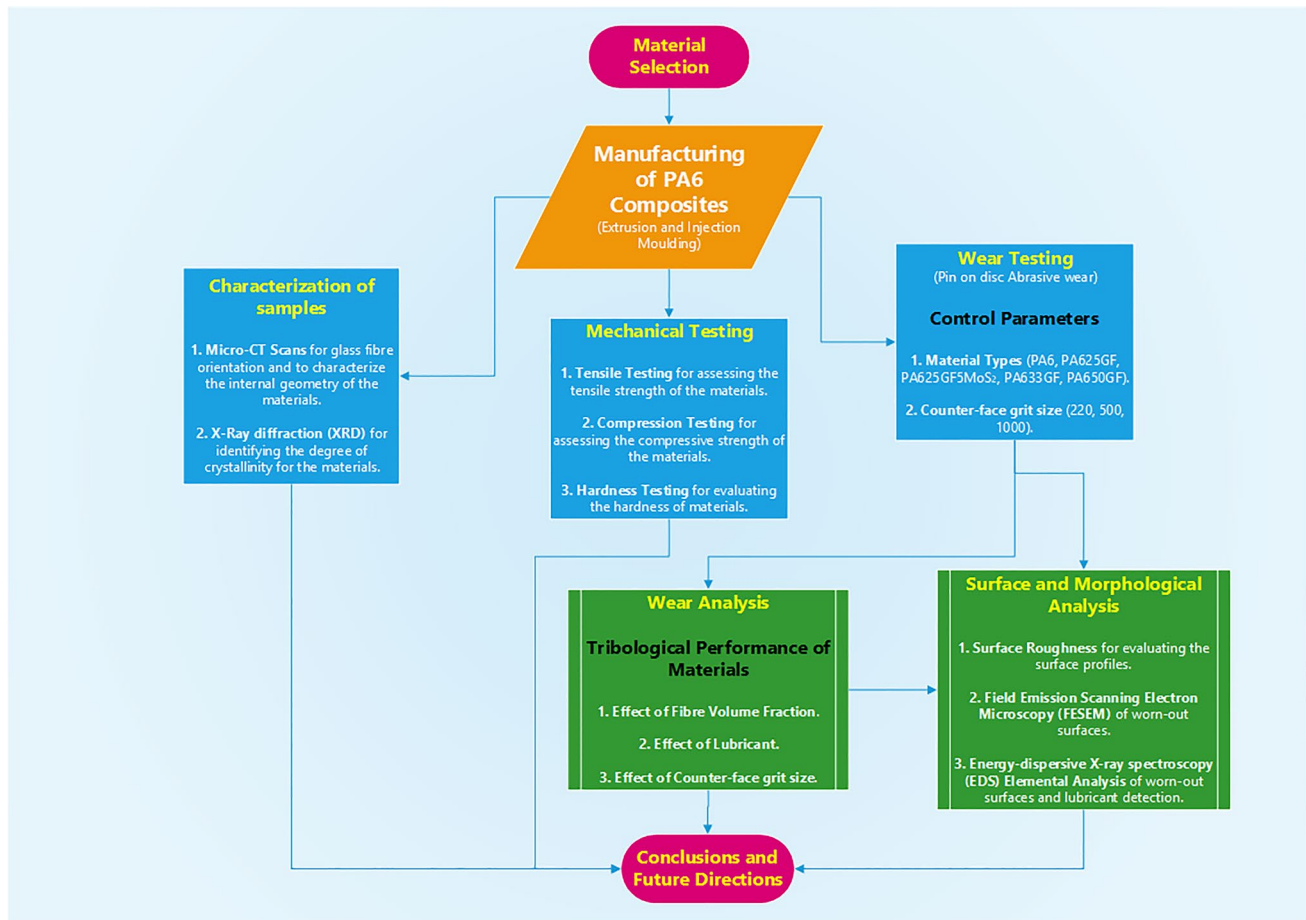
Keywords Wear resistance · Mechanical properties · Fibre volume fraction · Grit size · Wear performance · Man-made fibres · Composites · Wear behaviour · Polymer composites

Abbreviations

ASTM	American Society for Testing and Materials
CF	Carbon fibre
EDS	Energy-dispersive X-ray spectroscopy
FESEM	Field-emission scanning electron microscopy
FRP	Fibre reinforced polymer
GF	Glass fibre
GFR	Glass fibre reinforced
Micro-CT	Micro-computed tomography
MoS_2	Molybdenum disulphide
PA6	Polyamide 6
PEEK	Polyetheretherketone
PEI	Polyetherimide
PPS	Polyphenylene sulphide
PTFE	Polytetrafluoroethylene
PU	Polyurethane
SGF	Short glass fibres
SiC	Silicon carbide
TiO_2	Titanium dioxide
TPU	Thermoplastic polyurethane
UHMWPE	Ultra-high molecular weight polyethylene
W_s	Specific wear rate
X_c	Degree of crystallinity

1 Introduction

Friction is the primary phenomenon that takes place between the contacting members of devices and machinery. Frictional processes associated with the tear and wear of pairing members play a vital role in deteriorating the functional efficiency of these members. High wear rate and frictional coefficient are the major reasons that lead to reduced service life of vital elements such as vacuum

pumps, bearings and gears [1]. Moreover, in some extreme working environments, wear resistance and antifriction needs are higher, which majorly restrict the utilization of traditional thermoplastic materials in various sectors. Adhesion of the contacting member surfaces, crushing, cracking, tribo-chemical interactions that take place on the frictional surfaces and the abrasion of materials lead to the tribological wear of thermoplastic materials, as explained in various research works [2–5]. Hence, it is essential to investigate methods to enhance the tribological characteristics of polymeric materials. The methodologies that further enhance the tribological and abrasive properties of thermoplastic materials by transforming them into composite structures receive substantial scientific and commercial attention [1]. Currently, various inorganic and organic fibres are available as reinforcing materials for polymers and can be utilized in applications where abrasive resistance is of great necessity; for instance, seals, bushes, pump, conveyor belts, gears, chute liners and vanes, etc. [2, 3]. Glass fibre (GF) is amongst the most popular man-made fibre and is extensively utilized in different sectors such as: transportation, mining, sports equipment, automotive and aviation due to its distinct characteristics including low density, high compressive strength, and low cost [4].

Polymeric materials demonstrate distinct properties, in contrast to ceramics and metals, due to their relatively high strength to weight ratio and their viscoelastic behaviour characteristics [6–16]. Polymeric tribo-composite materials can be altered by incorporating reinforcements, filler materials and lubricants, in accordance with the predicted wear forms or situations [17–19]. Therefore, various parameters affect wear rates including the type of matrix, type of fibre, surface roughness, physical, mechanical and chemical characteristics of mating elements, contact kinematics and service conditions [20, 21]. These parameters are critical, specifically in the abrasive wear situation that takes place when stiff particles or hard surfaces glide on a soft material. The resulting surface grooving can lead to multiple folds of wear damage compared to adhesive form of wear [22, 23]. The filler materials, that improve the adhesive wear performance, may lead to extreme damage in abrasive mode of wear [24]. It is commonly anticipated that if there is an increase in rigidity and tensile strength of polymeric materials as a result of adding reinforcements, their resistance to wear should increase proportionally. Even though there are studies demonstrating that an optimal quantity of reinforcement is needed to achieve superior resistance to wear, the behaviour of the polymeric composites with improved mechanical characteristics exposed to abrasive form of wear is still questionable and unpredictable. Numerous researchers have investigated the improved abrasive wear performance of

polymers reinforced with fibres in comparison to neat polymeric materials [25–29]. Nonetheless, few research works have reported on the decrease of polymeric composites resistance to wear even when there is an increase in Young's modulus and hardness [20, 25]. The decrease in wear performance can be attributed to the operating conditions including sliding velocity, properties of the abrasive materials or the normal load applied, or the particular mechanical characteristics of the damaged material including fatigue behaviour [30] that all can increase the recurring ploughing influence on a stiff material. The resistance to abrasive wear of ultra-high molecular weight polyethylene (UHMWPE) composite materials reinforced with wollastonite fibre decreased as the amount of fibre surpassed 10% by weight [25]. On the other hand, the wear resistance characteristics of thermoplastic materials cannot be enhanced through the addition of short fibres if the form of wear is extremely abrasive [19].

In another study, Polyamide 6 (PA6) was reinforced with three different fibre volume fractions of short carbon fibres (CF) which were: 10%, 20% and 30%. When reinforcing PA6 with 20% of CF, the maximum resistance to wear was exhibited under the dry sliding wear state [31]. PA6 and polyphenylene sulphide (PPS) were reinforced with CF at three different weight fractions which were: 5%, 10% and 15% and the materials were tribo-tested. The results showed that there was a proportionate increase in resistance to wear with the increase in CF weight fraction, whereas there was a reduction in the coefficient of friction up to 10% of CF which increased with the increase of CF weight fraction [32]. Moreover, there was a proportional increase in wear rates with the increase in fibre content when polyurethane (PU) composite materials reinforced with short glass fibres (SGF) at 10%, 20%, 30% and 40% by weight were subjected to the abrasive form of wear [33]. The wear rate decreased with the increase of fibre content for Polyvinyl Pyrrolidone composite materials reinforced with Date Palm Leaf at 30% and 40% by weight fraction [34]. There was a proportionate increase in the wear rate and coefficient of friction with the rise in CF content at 5%, 10%, 15% and 20% by weight as a result of fibres aggregation for phenolic-CF composite materials [35]. The optimum tribological and mechanical characteristics were observed for paper-based frictional composite material reinforced with 10% by weight of short glass fibres [36]. Moreover, a similar observation was noticed for Polyetheretherketone (PEEK) composite materials comprising potassium titanate and short carbon fibres at 5%, 10%, 15% and 20% by weight fraction [37]. For Polyetherimide (PEI), the effect of increasing carbon fabric amount at 40%, 55%, 65%, 75% and 85% by weight fraction showed that the highest wear resistance in abrasive mode, reciprocating and adhesive wear forms were observed for composites reinforced with 65% by weight of carbon fabric [38–40]. The fabric amount, necessary for obtaining the

highest wear resistance and highest mechanical characteristics was not matching. Moreover, the amount of threshold changed for each wear form. The lesser weight fraction of fabric demonstrated being insufficient to act as an efficient wear barrier in the case of PEI, whereas higher weight fraction of fabric severely decreased the overall performance and resulted in higher wear and breaking of fibres due to the improper matrix wetting.

The main motivation of this research thus is elucidate the interactions between the contacting surfaces (Polyamide 6 and its glass fibre reinforced variations against Silicon carbide) with respect to grit size variations and material configuration variations. The abrasive wear behaviour of the injection moulded PA6 composites was investigated as a function of varying fibre volume fractions. The influence of grit size of a hard counter-face material (replicating a real-life application) on the wear performance of the selected materials was assessed. Additionally, the mechanical properties and surface roughness analysis of the manufactured samples were analysed. Besides, the morphological analysis of the worn-out surfaces was investigated. In light of the research gaps discussed in the review article by Moustafa et al. [1], the composites of three fibre volume fractions have been produced by injection moulding, and some combinations included Molybdenum disulphide (MoS$_2$) as a lubricant. The required wear, tensile, hardness and compression test specimens were prepared for assessing the influence of the compositions of different constituents on the tribological and mechanical performances of PA6 composites. The pin-on-disc abrasive tests under dry conditions were carried out using three different grit sizes for the counter-face material and the relationships between wear and mechanical behaviours were assessed based on the findings. Finally, the wear modes of the prepared materials are discussed.

2 Materials and Characterizations

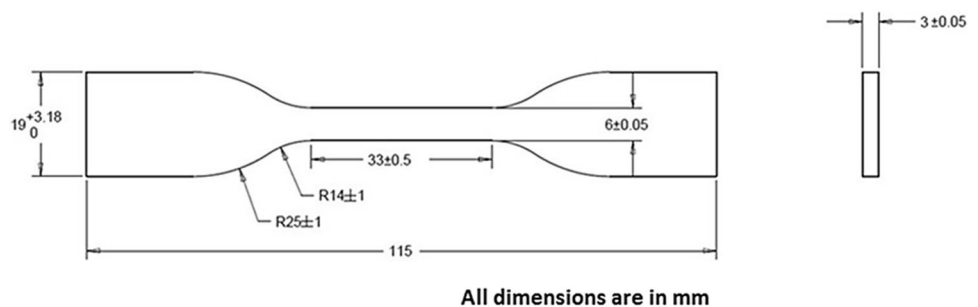## 2.1 Materials and Preparation

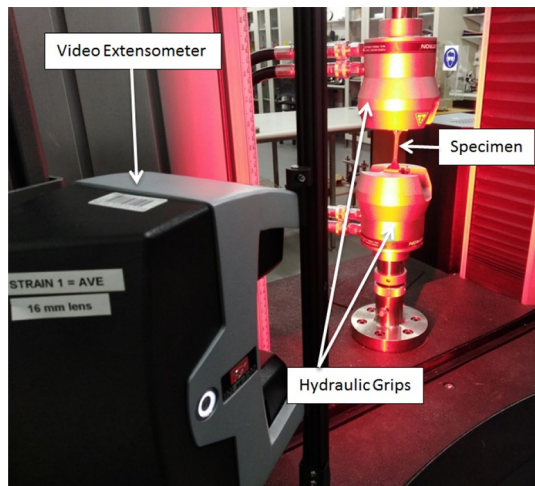In this research, the raw materials used were Polyamide 6 (PA6) as the matrix material and E-glass fibres as the reinforcement phase. The yield strength, flexural strength and specific gravity of PA6 were: 77.0 MPa, 92.0 MPa and 1.13, respectively, as supplied from Duromer (Australia). There are five different material compositions prepared which are: Pure PA6, PA625GF (PA6 + 25% by volume of E-glass fibres), PA625GF5MoS$_2$ [PA6 + 25% by volume of E-glass fibres + 5% by weight of the lubricant Molybdenum disulphide (MoS$_2$)], PA633GF (PA6 + 33% by volume of E-glass fibres) and PA650GF (PA6 + 50% by volume of E-glass fibres). The injection moulding process was used to manufacture the different material compositions by using HXF 168 by NINGBO HAIXING PLASTICS MACHINERY moulding machine. The real-life application of the manufactured pure thermoplastics, lubricated thermoplastics and fibre reinforced thermoplastic materials is targeting the mining industry. Different moulds were used to obtain samples of the required geometries for tensile, compression, roughness, density measurement, wear testing and morphological analysis.

2.2 Mechanical Testing of Materials

The mechanical properties of the materials were evaluated using an INSTRON model 5900R 5584 universal testing machine from Germany, under normal ambient temperature conditions. The load cell capacity was 10 KN and the type of grippers used was self-aligning hydraulic grips. To remove moisture from the samples, they were subjected to drying at 60 °C in a drying chamber for 24 hours prior to the tension test. The tensile testing was carried out in accordance with ASTM standard D638-10 [41] at a constant cross head speed of 5 mm/min and a gauge length of 33 mm. The data were acquired using a video extensometer instead of the crosshead displacement to overcome the slippage effect between the sample and grips. An assessment of each material configuration involved analysing five distinct specimens, with the mean values of the measured parameters recorded for each. The geometry of the tensile samples is presented in Fig. 1 and the tensile testing setup is shown in Fig. 2. Additionally, the compression testing of materials was carried out in accordance with the standard ASTM D 695 [42] for the

Fig. 1 Geometry of the tensile specimens

All dimensions are in mm

Fig. 2 Testing Setup of Tensile Specimens using the INSTRON Universal Testing Machine

Fig. 3 Wear testing setup using the 5135 Abraser tribometer device

Fig. 4 Schematic diagram for abrasive wear of pin samples against SiC abrasive paper bonded disc

compression testing of plastic materials, using the same universal testing machine. The height and diameter of the dried rod-shaped samples were 15 mm and 10 mm, respectively. The crosshead speed was set at 1.3 mm/min. Likewise, five samples were tested per configuration and the average results were recorded. Moreover, shore D hardness was measured using an INSTRON tester, following ASTM D2240-15. The scale ranges from 0 to 100, with lower values indicating lower hardness. Specimens were 10 mm in diameter and 15 mm in height. Samples were cleaned with alcohol before testing to ensure accurate readings. The test was done at 25 °C and 50% relative humidity, with a 1-second delay before recording readings and ten measurements per sample were averaged.

2.3 Wear Testing of Materials

Prior to the wear testing of materials, the density of the samples was assessed using a density kit, following the Archimedes principle and the testing procedures of ASTM 792 standard for density calculation of plastic materials [43]. The mass of each sample was recorded using a weighing scale of 0.1 mg scale value, in two conditions; air medium and water medium. Five samples of each material configuration were assessed and the average values of densities were reported. The tribological properties of the polymeric samples were carried out by using the pin-on-disk tribometer, rotary platform abrader 5135, as presented in Fig. 3. The geometry of the sample used for abrasion was a rod of 15 mm height and 10 mm diameter which were checked using a Vernier Caliper with a scale resolution value of 0.01 mm. An illustration of the wear testing configuration showing the pin sample and the silicon carbide (SiC) grinding paper as the counter-face material is presented in Fig. 4.
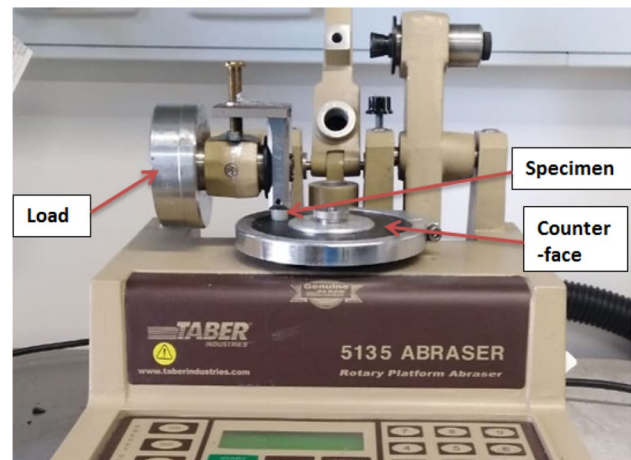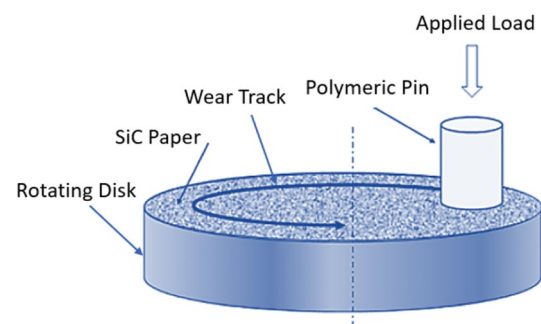
The counter-face material used for the abrasion testing was SiC which was provided by Struers, and the polymeric pins were abraded against three different grit sizes which were: 220, 500 and 1000, which replicate coarse grit, medium grit and fine grit sizes, respectively. Table 1 lists the characteristics of the counter-face materials used for abrasion. The outside diameter of SiC papers was 102 mm and the track diameter was kept at 82 mm in the abrasion experiments.

The abrasion testing of polymeric samples was performed as per the ASTM G99-17 standard for abrasion testing of materials in a pin on disk format [44]. Prior to wear testing, the polymeric specimens were cleaned from dirt and foreign particles using ethanol, followed by being dried in the oven at 50 °C for six hours, in order to obtain a similar surface finish for the samples. The mass of all samples was measured before and after wear testing using a balance scale of 0.1 mg scale resolution value. The pin samples were placed securely in the specimen's holder while ensuring that the samples meet the required contacting conditions by being perpendicular to the rotating grinding paper. The abrading

Table 1 Properties of the counter-face materials

Serial	Counter-face material	Grit size (European FEPA)	Particle size (μm)
1	SiC	220	68
2	SiC	500	30
3	SiC	1000	18

velocity and applied force were set at 72 rpm (0.31 m/s) and 10 N, respectively. The abrading distance was set at 257.48 m for all samples by controlling the revolutions count for each experiment. A new abrasive paper was used for each sample. Five samples were examined for each material composition and the average mass loss values were calculated in order to evaluate the specific wear rate of the materials (W_s) [1]. The abrasion test was performed at ambient conditions (25 ± 2 °C) without any disruptions. After completion of the abrasion test, the sample was removed, cleansed of any wear debris through the use of ethyl alcohol, and subsequently dried, prior to the measurement of the final mass.

The mass loss of polymeric specimens was evaluated according to Eq. (1), as follows:

$$\Delta m = m_i - m_f \, [\text{mg}] \tag{1}$$

where, Δm is the mass loss of the specimen, m_i is the initial mass of the specimen and m_f is the final mass of the specimen after the abrasion testing.

The wear amount was converted from mass loss to volumetric loss and Eq. (2) expresses (ΔV) as the ratio of mass loss to the calculated density of the materials.

$$\text{Volumetric loss } (\Delta V) = \frac{\text{Mass loss, (g)}}{\text{Density, (g.cm}^{-3})} \times 1000 \, [\text{mm}^3] \tag{2}$$

Through the utilization of Eq. (3), the calculated data obtained from the wear test enables the determination of the specific wear rate W_s.

$$W_s = \Delta V / F_N L \, [\text{mm}^3/\text{N.m}] \tag{3}$$

where L is the abrading distance in meters, ΔV is the volumetric loss in mm³ and F_N is the applied load in newtons.

2.4 Roughness Testing of Materials

The surface profiles of the polymeric pins were evaluated using the 3D digital profilometer Olympus DSX1000 across the worn-out surface of the samples. The surface texture parameters, Arithmetical mean height (Ra), Mean width of the profile elements (Rsm) and Maximum height of profile (Rz) were used to indicate the surface roughness pin
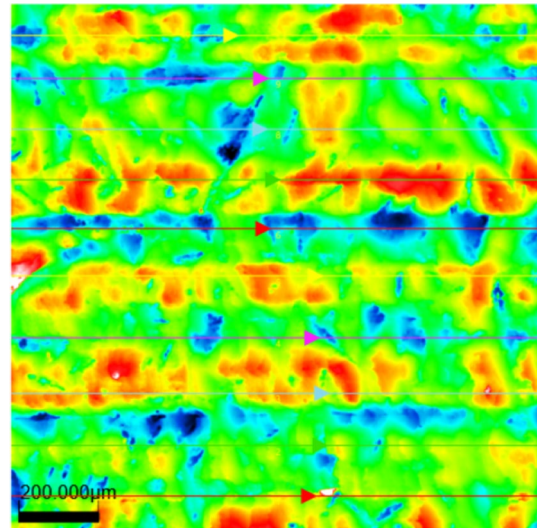
Fig. 5 Representation of the roughness lines drawn for assessing the surface roughness parameters of the polymeric pin samples

samples that were subjected to abrasive wear. The profile roughness for each sample was assessed by measuring the roughness values across ten equally spaced lines, as seen in Fig. 5, on the surface of each sample and the average results were recorded.

2.5 Micro-CT Analysis of Materials

The specimens were subjected to micro-CT scanning using the SkyScan 1272 instrument from Bruker (Belgium), which enabled evaluation of fiber orientation and distribution. The following parameters were used during acquisition: 1.25 μm voxel size, 111 uA current, 70 kV voltage, 2.175 seconds of exposure time, 0.5 mm Al filter, 2x2 binning, frame averaging of 2, and a rotation step of 0.18 degrees around the specimen's full 360-degree rotation. The micro-CT data was reconstructed using InstaRecon (from InstaRecon, USA) and NRecon (Version 1.7.4.6, from Bruker, Belgium) through back-projection algorithm, with ring artifact reduction and correction for beam hardening. Visualization of the data were achieved via CTVox from Bruker, Belgium.

2.6 X-Ray Diffraction (XRD) Analysis

The X-ray diffraction (XRD) analyses were performed using a Bruker D8 Advance instrument equipped with Cu Kα2 radiation over a 2θ range of 10˚ to 60˚. The measurements were conducted in fixed time mode with a step size of 0.02˚ per minute. The crystalline and amorphous components of the materials were distinguished and the crystallinity degree (W_s) was determined using DIFFRAC.EVA Version 5.1.

2.7 Morphological Analysis of Worn-out Surfaces

The morphologies of the worn-out surfaces of polymers and polymeric composite materials were assesseusing JEOL 7100 field emission scanning electron microscope (FESEM). The tribological tested polymers and composites were plasma cleaned and the worn-out surfaces for observation were platinum coated with a layer of 15 nm thick, to render them electrically conductive. The specimens' worn surfaces were positioned facing upwards on a standard FESEM stub affixed with double-sided carbon tape. During FESEM imaging, parameters such as accelerating voltage (kV) and probe current (A) were fine-tuned to produce high-quality images devoid of any sample charging or surface degradation artefacts. Based on our findings, optimal images were obtained by employing a 10 kV accelerating voltage and 8 A probe current. Different magnifications were used to capture a representative view of the worn surfaces.

3 Results and Discussion

3.1 Mechanical Performance of Materials

The subsequent section of this study details and analyses the mechanical properties of both pure polymers and fibre-reinforced polymers, which were determined through a variety of testing methods, including wear testing, hardness testing, compression testing and tensile testing.

#### 3.1.1 Tensile and Hardness Behaviours of Materials

Figure 6 illustrates the tensile properties of PA6 and its composites, which includes 25%, 33%, and 50% by volume of glass fibres. The data indicates that PA650GF has the highest Young's modulus among the materials tested. Moreover, PA650GF exhibits a tensile strength 231% greater than the lowest-performing material, PA6. These findings suggest that an increase in fibre volume fraction leads to an increase in the composite materials' stiffness, Young's modulus, which is consistent with the rule of mixtures theory. Additionally, it can be observed that that the inclusion of a 5% MoS_2 lubricant in PA625GF results in an average increase of 14% in Young's modulus when compared to the absence of the lubricant. The mean values of Shore D hardness readings for specimens with different formulations has been measured. It is anticipated that an increase in the number of rigid components within a relatively softer component would result in higher hardness values. Several factors influence the hardness values in fibre-reinforced thermoplastics, including fibre size, type, volume fraction, and the adhesion strength between the matrix and the fibre. The contribution of the fibre volume fraction to hardness was confirmed through the hardness testing results. These results demonstrate that the thermoplastic composite materials exhibited higher hardness values compared to the plain polymers. The mean hardness values for PA6, PA625GF, PA625GFMoS2 and PA633GF were 74.9, 82.8, 85.3 and 86.5, respectively. Notably, the 50% filled glass fibre-reinforced thermoplastic materials exhibited the highest hardness values, reaching as high as 93.3 Shore D. This is attributed to the rigid structure of the fibres and their higher volumetric fraction in the composite, which contribute to the enhanced hardness properties.

3.1.2 Compressive Behaviour of Materials

Figure 7 depicts the compressive strength of two polymer candidates and PA6 reinforced variations. The results indicate that PA6 demonstrates 91% greater compressive strength than TPU at 30% strain. Furthermore, the compressive strength values of glass fibre-reinforced PA6 display a direct correlation with fibre volume fraction, with PA6 reinforced with 50% glass fibres by volume exhibiting

Fig. 6 Young's modulus for PA6 and glass fibre reinforced PA6 at different fibre volume fractions
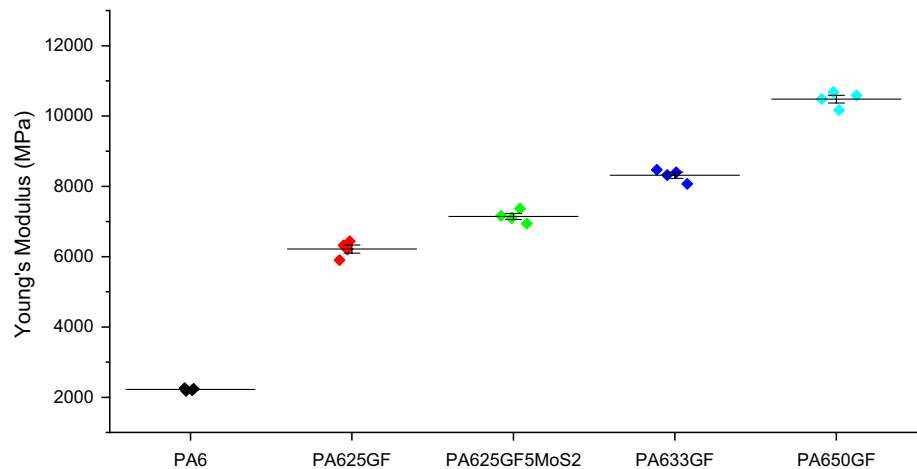
Fig. 7 Compressive strength for polymeric materials and variations of glass fibre reinforced PA6
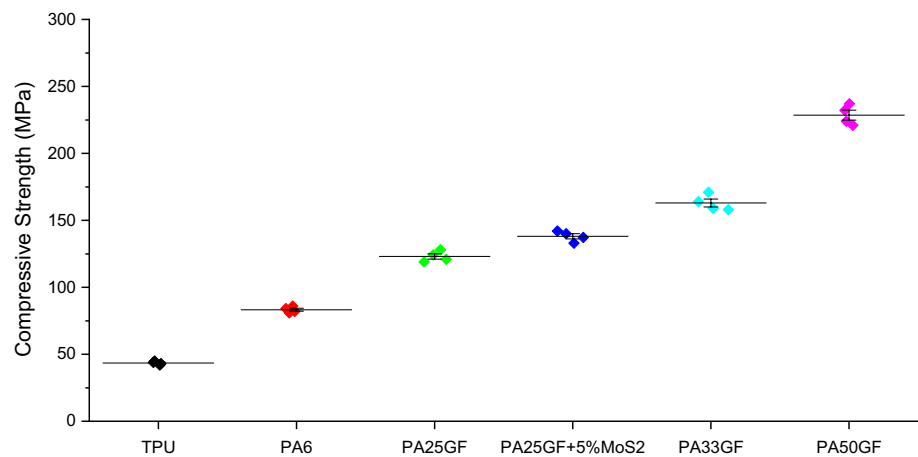
higher compressive strength than PA633GF and PA625GF by 40% and 86%, respectively. Additionally, the inclusion of a lubricant marginally increased PA6's compressive strength by 11.7%. These findings align closely with the tensile test results of the materials, as previously discussed.

3.1.3 Wear Behaviour of Materials

Tables 2, 3, and 4 present the mass loss data for neat polymers and PA6 composites, subjected to varying configurations of Silicon carbide grinding paper counter-face with grit sizes 1000, 500, and 220, respectively. The mechanical and wear characteristics of polymeric composite materials are greatly influenced by the type, size, and shape of the filler, as well as its chemical treatment. For instance, shorter fibre lengths may decrease the load carrying capacity of fibres and lead to high wear rates, whereas longer fibre lengths may cause pull-out of the fibres and increase wear rates. Therefore, the use of fibres shorter than the critical length was pursued to improve stress transfer efficiency.

In order to evaluate the wear characteristics of the composite specimens, both mass loss and volume loss measurements were taken. Subsequently, the mass loss data was converted to wear volume (ΔV) using the average values of densities recorded for the five specimens examined per configuration. The densities of the fibre-reinforced composite

materials and their corresponding wear amounts, as quantified by both volumetric and mass loss measurements, are presented in Table 5, with respect to the three grit sizes of the counter-face material used.

The specific wear rate of PA6 was investigated with the addition of three different fibre volume fractions (25%, 33%, and 50%) and glass fibre at 25% volume fraction, along with 5% lubricant material MoS_2. The samples were subjected to three different grit sizes of SiC counter-face grinding papers, and the results were presented in Figure 8. The addition of glass fibres was found to decrease the wear resistance of the composite materials in all cases. The specific wear rate rose with the increase of fibre volume fraction, possibly due to the increased rigidity of the structure at higher fibre fractions, leading to increased abrasive wear. The wear rate of PA650GF was found to be the highest, with specific wear rates against SiC of grit size 220, 500, and 1000 being 163%, 161%, and 178% higher than that of pure PA6, respectively. These results are partially consistent with the findings of Palabiyik et al. [45], who concluded that the addition of glass fibres was not effective in reducing the wear rate of high-density polyethylene and polyamide 6 polyblends. Additionally, the incorporation of 5% MoS_2 led to a significant decrease in the wear rate, with a reduction of 18.84% observed when comparing the wear rates of PA625GF+5% MoS_2 and PA625GF.

Table 2 Mass loss measurements of the polymeric and composite samples against SiC counter-face of grit size 1000

Sample	Mass loss (mg)					Mean value (mg)
PA50GF	4.0	4.0	4.0	5.0	4.0	4.2
PA33GF	5.0	5.0	6.0	5.0	6.0	5.4
PA25GF5MoS$_2$	6.0	7.0	6.0	6.0	7.0	6.4
PA25GF	8.0	8.0	9.0	8.0	9.0	8.4
PA6	10.0	10.0	11.0	10.0	10.0	10.2

Table 3 Mass loss measurements of the polymeric and composite samples against SiC counter-face of grit size 500

Sample	Mass loss (mg)					Mean value (mg)
PA6	18.0	19.0	19.0	20.0	19.0	19.0
PA33GF	25.0	25.0	26.0	25.0	26.0	25.4
TPU	25.0	25.0	26.0	24.0	28.0	25.6
PA25GF5MoS$_2$	34.0	31.0	32.0	30.0	31.0	31.6
PA25GF	39.0	37.0	39.0	38.0	37.0	38.0
PA50GF	37.0	41.0	42.0	45.0	43.0	41.6

Table 4 Mass loss measurements of the polymeric and composite samples against SiC counter-face of grit size 220

| Sample	Mass loss (mg)					Mean value (mg)
PA50GF	211.0	204.0	212.0	209.0	215.0	210.2
PA33GF	126.0	129.0	121.0	126.0	128.0	126.0
PA25GF5MoS$_2$	190.0	189.0	191.0	192.0	188.0	190.0
PA25GF	201.0	197.0	205.0	202.0	199.0	200.8
PA6	48.0	45.0	49.0	51.0	47.0	48.0

Table 5 Density and wear amount of PA6 and PA6 composite samples

Sample	Density (ρ) [g/cm^3]	Grit size #220		Grit size #500		Grit size #1000	
		Mass loss (Δm) [mg]	Volume loss (ΔV) [mm^3]	Mass loss (Δm) [mg]	Volume loss (ΔV) [mm^3]	Mass loss (Δm) [mg]	Volume loss (ΔV) [mm^3]
PA6	1.128	210.200	186.340	19.000	16.840	4.200	3.720
PA33GF	1.319	126.000	95.520	25.330	19.200	5.400	4.090
PA25GF + 5%MoS$_2$	1.331	190.000	142.740	33.330	25.040	6.400	4.810
PA50GF	1.533	200.800	130.980	41.670	27.180	8.400	5.470
PA25GF	1.286	48.000	37.320	40.000	31.100	10.200	7.930

PA6 and PA6 reinforced compositions showed greater wear rates, specifically against 220 abrasive grit size, than these against 500 and 1000 abrasive grit sizes. The penetration depth, namely wear depth was significantly higher for the materials which were abraded against 220 grit size paper than the higher grit sizes. Therefore, PA6 and PA6 reinforced compositions demonstrated wear sensitivity to these adverse contacting conditions. The main aspects of two-body abrasive wear of thermoplastics are reflected in micro-cutting and micro-ploughing forms. In the micro-ploughing form, a shallow groove was created due to continuous loading. In the micro-cutting form, long, curled ribbon-like particles were generated. Therefore, the wear of polyamide compositions was dominated by micro-ploughing because of deep penetration of the brittle SiC particles and material being transferred on either face. The fibrils were adhering to the counter-face during micro-cutting. The clogging of the SiC abrasive papers with wear debris and fibrils may also have an influence on the specific wear rate of the materials.

In the case of 500 and 1000 abrasive grit sizes, the abrasivity was decreased after repeated abrading and clogging. This expresses why substantial fluctuations in the specific wear rates were not detected in 500 and 1000 grit size papers. In two-body abrasive wear, the abrasive particles were involved in micro-ploughing while the remainder of the abrasive particles are responsible of micro-cutting [46]. The angle of the abrasive particles with respect to softer surfaces is said to be controlling the material deformation. The abrasive wear rate of polymers is proportional to $\frac{1}{\sigma_u \varepsilon_u}$ where ε_u is the elongation at break and σ_u is the tensile break strength [47]. The less values of $\frac{1}{\sigma_u \varepsilon_u}$ lead to reduced wear rates. Accordingly, PA33GF showed improved wear resistance than PA50GF. The elongation at break of PA50GF is less than that of the other fibre fractions and it is one of the main controlling factors for resisting wear, particularly in severe conditions. Hence, under adverse conditions, as against 220 grit size papers, PA6 and PA6 reinforced compositions are more susceptible to wear due to their mechanical characteristics.

Fig. 8 Average specific wear rate for polymers and their fibre reinforced variations for three different grit sizes of SiC counter-face
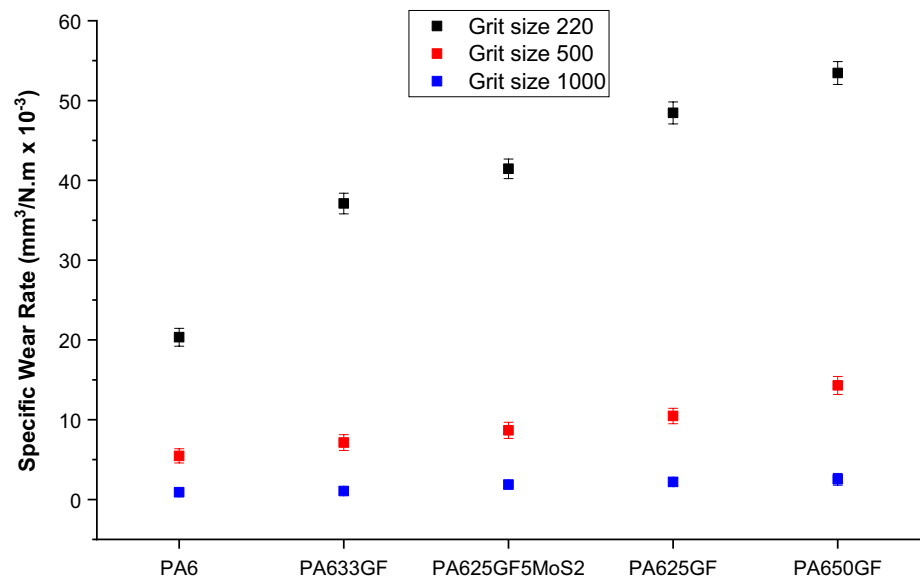

The lubricant was significant in minimizing the friction at interfaces in relative motion, hence minimizing the wear rate and increasing the lifetime of structures subjected to abrasive wear. The thermal resistance of composites is a critical factor affecting their friction and wear properties. During friction, heat is generated, particularly under dry sliding conditions, and in the absence of lubrication, the generated heat cannot be dissipated. Consequently, composites are more prone to degradation in the presence of frictional heat, and those with higher thermal stability exhibit greater resistance to such damage. In our current research, we have determined that PA625GF+5% MoS_2 composites exhibit excellent thermal stability, which is advantageous for their wear properties. Moreover, the PA625GF+5% MoS_2 samples exhibit higher hardness, indicating that they have better load-carrying capacity and can prevent PA6 from wearing off. This improvement in wear resistance because of the incorporation of MoS_2 is consistent with previous studies [48–51]. Additionally, among the three fibre volume fractions used to reinforce PA6, we found that 33% glass fibre content by volume was the optimal percentage for resisting wear, with the specific wear rate of PA633GF being 30.59% and 44.07% less than that of PA625GF and PA650GF, respectively. Abrasive wear causes the surfaces of the counter-face materials to become relatively rough compared to the unworn side surfaces of SiC grinding papers. During sliding between the counter-face and candidate polymers, the adhesion between the two surfaces at the original interface is strong enough to impede sliding motion, leading to tearing at the interfaces within the polymeric specimens. Consequently, a coherent thin film of each specimen is deposited on the counter-face material in the wear track. Subsequent motion of the polymeric specimen over this thin layer removes the transferred film, and a new layer is deposited. This process continues until the surfaces of the polymeric specimens are gradually worn away. The results indicate that the specific wear rate of materials decreases as the grit size of the counter-face increases. This finding is consistent with previous research that suggests the abrasive wear resistance of polymer composites is proportional to their rigidity or fibre volume fraction in fibre-reinforced composite systems, as reported in the literature survey [52–54].
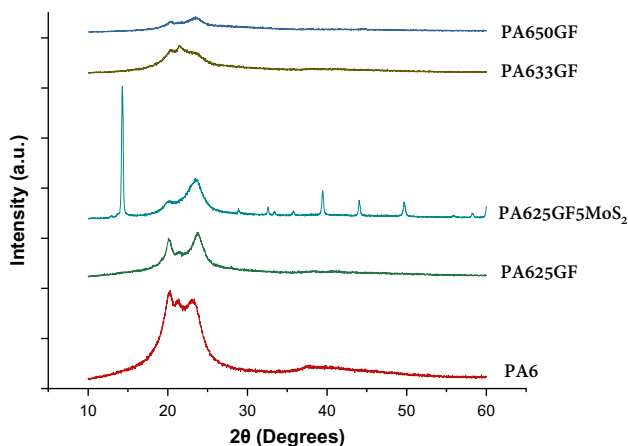
3.2 Micro-CT Analysis of Materials

The micro-CT, as a non-destructive technique was carried out to visualize and characterize the internal geometry of the thermoplastics and thermoplastic composites. It was used to investigate fibre alignment, fibre distribution, the existing voids and the effect of the injection flow in the manufactured composites. Besides, it was carried out to check if there are structural changes due to the applied moulding conditions. Figure 9 presents 3D tomogram images of the polymeric reinforced specimens, showing the randomly distributed fibres of varying lengths. The fibre phase is represented in red colour, while the matrix phase is represented in white. The elevation views of the images in Fig. 9 represent the section views of specimens, while the top views of the images in the same figure represent the top surfaces of the specimens. The direction of glass fibres is perpendicular to the loading direction of the injection moulding process. Notably, the images reveal that the injection moulding process resulted in a close packing of the composites, thereby achieving uniform fibre distribution without any agglomerates. Additionally, the images demonstrate that the composites exhibited negligible voids.

Fig. 9 Tomogram 3D image visualisations of the central portion of the plain polymeric specimens; each subset representing approximately one third of the specimens' volumes imaged; (PA625GF, PA625GF+5MoS$_2$, PA633GF and PA650GF)
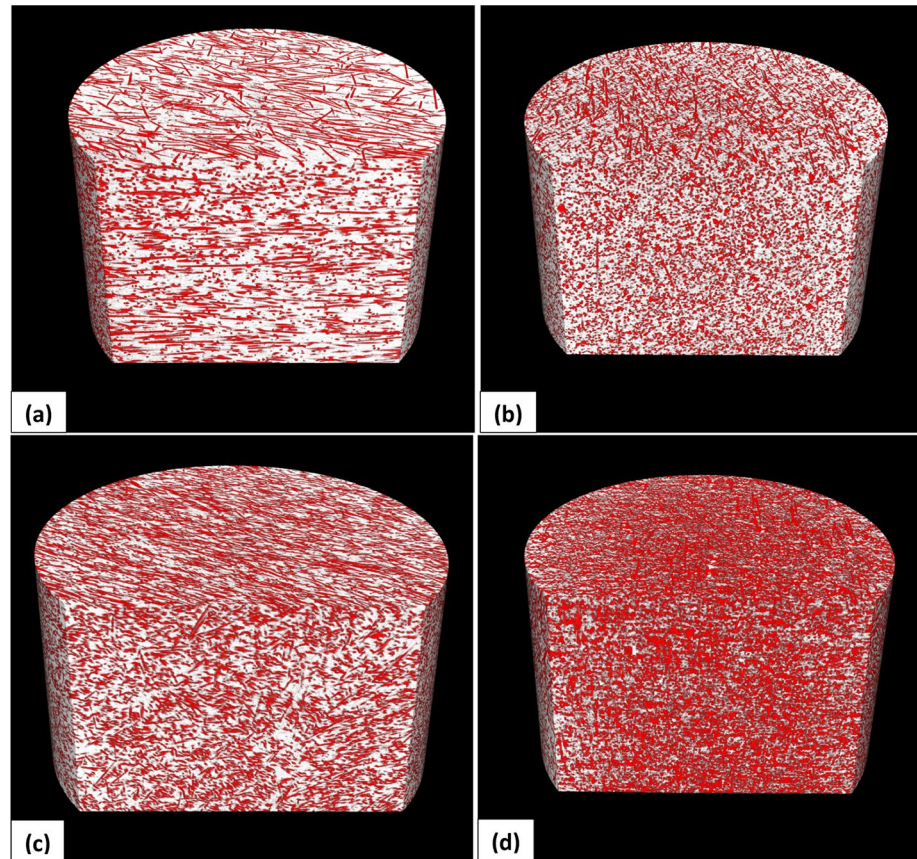
3.3 XRD Analysis of Materials

X-ray diffraction (XRD) analyses were employed to determine the crystallographic properties of both PA6 and PA6 composite materials, as well as to evaluate the influence of the resulting degree of crystallinity on the materials' wear resistance. The XRD results are presented in Fig. 10,

showing characteristic peaks of PA6 at $2\theta = 20.8°$ (200) and $22.9°$ (202, 002).

Table 6 displays the degree of crystallinity of the investigated materials. The addition of glass fibres was observed to decrease the intensity of the characteristic peaks, while the introduction of MoS$_2$ resulted in a noteworthy rise in the crystallinity of the materials, increasing from $X_c = 40.52$ to $X_c = 52.38$. This rise in crystallinity corresponds to a reduction in the specific wear rates.
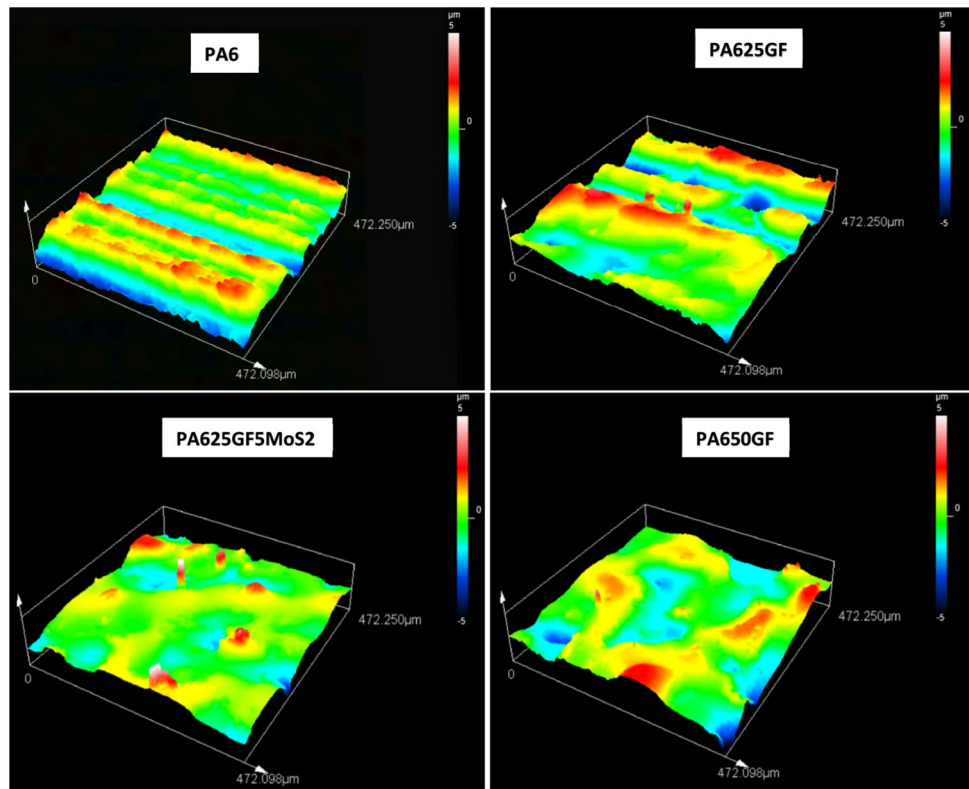
3.4 Surface Roughness of Worn-Out Surfaces

The worn-out surfaces of polymers and their composites in the analysed scenarios have been assessed by measuring the roughness parameter Ra across ten profile lines on each

Fig. 10 X-ray diffraction (XRD) patterns of PA6 and PA6 composites

Table 6 Degree of crystallinity of PA6 and PA6 composite materials

Serial	Sample code	Crystallinity degree (Xc%)
1	PA6	47.03
2	PA625GF	40.52
3	PA633GF	37.81
4	PA650GF	33.39
5	PA625GF5MoS$_2$	52.38

Fig. 11 Height maps of the materials (PA6, PA625GF, PA625GF5MoS$_2$ and PA650GF) against SiC, grit size 1000

sample, as shown in Fig. 5. The height maps of the different surfaces worn-out by SiC counter-face of grit size 1000 are displayed in Fig. 11. The line roughness parameters for the worn-out surfaces of PA6 against SiC of grit sizes 1000, 500 and 220 are displayed in Tables 7, 8 and 9, respectively.

Additionally, the line roughness parameters for the worn-out surfaces of the optimum reinforced variation in terms of wear performance, PA633GF, against SiC of grit sizes 1000, 500 and 220 are displayed in Tables 10, 11 and 12, respectively.

Table 7 Surface roughness parameters of PA6 against SiC of grit size 1000

Measurement number	Rp[μm]	Rv[μm]	Rz[μm]	Rc[μm]	Rt[μm]	Ra[μm]	Rq[μm]	Rsk	Rku	Rsm[μm]
1	1.021	0.667	1.688	0.545	1.688	0.241	0.3	0.503	2.869	49.26
2	0.827	1.606	2.433	0.79	2.433	0.32	0.419	0.786	4.049	71.21
3	1.646	0.923	2.568	0.751	2.568	0.262	0.345	0.778	5.13	47.65
4	1.205	0.585	1.791	0.724	1.791	0.194	0.26	1.253	5.192	71.21
5	1.073	1.606	2.679	1.178	2.679	0.284	0.385	0.934	5.531	136.6
6	1.333	0.541	1.875	0.691	1.875	0.219	0.28	1.004	5.317	48.39
7	1.06	0.93	1.99	0.557	1.99	0.241	0.312	0.042	3.125	42.25
8	0.873	0.977	1.85	0.591	1.85	0.221	0.293	0.611	3.722	72.32
9	0.622	1.107	1.729	0.493	1.729	0.178	0.233	0.708	4.995	54.19
10	0.726	0.895	1.621	0.507	1.621	0.165	0.221	0.021	4.405	54.73
Average	1.039	0.984	2.022	0.683	2.022	0.232	0.305	0.174	4.434	64.79
Max	1.646	1.606	2.679	1.178	2.679	0.32	0.419	1.253	5.531	136.6
Min	0.622	0.541	1.621	0.493	1.621	0.165	0.221	0.934	2.869	42.25
Range	1.023	1.065	1.058	0.684	1.058	0.154	0.199	2.188	2.663	94.39
σ	0.303	0.374	0.389	0.203	0.389	0.048	0.064	0.782	0.953	27.54
3σ	0.91	1.123	1.167	0.61	1.167	0.143	0.191	2.346	2.859	82.63
Sum	10.39	9.838	20.22	6.828	20.22	2.324	3.047	1.74	44.34	647.9

Table 8 Surface roughness parameters of PA6 against SiC of grit size 500

Measurement number	Rp[μm]	Rv[μm]	Rz[μm]	Rc[μm]	Rt[μm]	Ra[μm]	Rq[μm]	Rsk	Rku	Rsm[μm]
1	5.013	2.726	7.739	1.865	7.739	1.29	1.656	0.752	2.933	88.322
2	2.744	1.741	4.485	3.314	4.485	0.925	1.077	0.511	2.151	122.09
3	2.117	2.006	4.123	2.09	4.123	0.76	0.938	0.14	2.662	75.47
4	1.301	2.426	3.727	1.885	3.727	0.53	0.675	-0.732	4.034	70.421
5	1.33	1.397	2.726	1.397	2.726	0.478	0.57	-0.18	2.425	68.126
6	1.155	0.796	1.951	0.979	1.951	0.388	0.458	0.13	2.112	85.45
7	2.21	1.642	3.852	1.253	3.852	0.412	0.549	0.751	5.094	46.467
8	1.405	1.44	2.846	1.315	2.846	0.446	0.561	0.33	2.692	35.178
9	5.523	2.336	7.858	4.784	7.858	1.405	1.879	1.371	4.222	103.075
10	5.648	4.181	9.83	7.813	9.83	1.968	2.378	0.498	2.467	120.778
Average	2.845	2.069	4.914	2.669	4.914	0.86	1.074	0.357	3.079	81.538
Max	5.648	4.181	9.83	7.813	9.83	1.968	2.378	1.371	5.094	122.09
Min	1.155	0.796	1.951	0.979	1.951	0.388	0.458	0.732	2.112	35.178
Range	4.493	3.385	7.879	6.834	7.879	1.579	1.92	2.103	2.982	86.912
σ	1.834	0.934	2.625	2.141	2.625	0.535	0.67	0.573	1.012	28.73
3σ	5.503	2.803	7.874	6.423	7.874	1.604	2.01	1.72	3.037	86.191
Sum	28.445	20.692	49.137	26.695	49.137	8.601	10.742	3.572	30.791	815.376

Table 9 Surface roughness parameters of PA6 against SiC of grit size 220

Measurement number	Rp[μm]	Rv[μm]	Rz[μm]	Rc[μm]	Rt[μm]	Ra[μm]	Rq[μm]	Rsk	Rku	Rsm[μm]
1	2.168	2.035	4.203	3.837	4.203	0.803	0.96	0.281	2.437	177.823
2	2.026	2.44	4.466	2.424	4.466	0.773	0.986	0.171	2.553	139.925
3	2.037	1.953	3.991	2.063	3.991	0.793	0.957	0.319	2.201	74.041
4	2.792	1.817	4.608	2.634	4.608	0.871	1.056	0.392	2.619	128.647
5	3.006	1.908	4.914	3.337	4.914	1.002	1.2	0.545	2.385	131.007
6	2.356	1.773	4.129	4.129	4.129	0.894	1.102	0.263	2.276	300.569
7	2.451	2.417	4.869	3.795	4.869	0.96	1.174	-0.157	2.482	295.454
8	2.417	2.227	4.644	1.68	4.644	0.945	1.124	-0.086	2.336	339.124
9	4.03	3.025	7.056	2.824	7.056	1.334	1.631	0.003	2.36	152.645
10	3.223	2.315	5.537	3.185	5.537	1.067	1.293	0.064	2.387	237.623
Average	2.651	2.191	4.842	2.991	4.842	0.944	1.148	0.179	2.404	197.686
Max	4.03	3.025	7.056	4.129	7.056	1.334	1.631	0.545	2.619	339.124
Min	2.026	1.773	3.991	1.68	3.991	0.773	0.957	0.157	2.201	74.041
Range	2.005	1.252	3.065	2.449	3.065	0.561	0.675	0.701	0.417	265.083
σ	0.629	0.38	0.899	0.808	0.899	0.167	0.202	0.222	0.125	89.445
3σ	1.886	1.141	2.696	2.423	2.696	0.5	0.606	0.666	0.374	268.334
Sum	26.507	21.91	48.417	29.908	48.417	9.442	11.483	1.795	24.036	1976.857

The surface roughness parameters in Tables 7, 8 and 9, show an increase in roughness with the increase in the wear volume which is attributed to the decrease in the grit size of the counter-face material. When increasing the grit size of the counter-face material to 1000, gradual flattening of the worn-out surface was observed during the abrasion, which is indicated by the reduction of surface roughness parameters to as low as (Ra = 0.232 μm, Rz = 2.02 μm and Rsm = 64.79 μm) as a result of surface smoothness. The same observation can been deducted out of the surface roughness parameters in Tables 10, 11 and 12, where the roughness values

Table 10 Surface roughness parameters of PA633GF against SiC of grit size 1000

Measurement number	Rp[μm]	Rv[μm]	Rz[μm]	Rc[μm]	Rt[μm]	Ra[μm]	Rq[μm]	Rsk	Rku	Rsm[μm]
1	1.353	1.633	2.986	2.222	2.986	0.626	0.731	− -0.493	2.064	131.1
2	2.268	1.225	3.493	2.122	3.493	0.444	0.619	0.409	4.442	188.1
3	1.646	1.203	2.849	1.181	2.849	0.447	0.578	0.352	3.011	67.08
4	0.706	0.768	1.474	0.853	1.474	0.249	0.306	0.144	2.574	107.3
5	3.319	2.059	5.378	3.392	5.378	0.593	0.822	0.85	5.809	121.6
6	1.336	2.517	3.852	1.849	3.852	0.487	0.674	− 1.37	5.695	112.7
7	0.999	1.889	2.888	0.962	2.888	0.54	0.682	− 0.686	2.842	114.5
8	1.993	3.087	5.08	3.452	5.08	0.854	1.057	− 0.18	2.532	148.4
9	1.422	1.69	3.112	1.32	3.112	0.51	0.668	− 0.642	3.218	87.26
10	0.871	0.79	1.661	0.994	1.661	0.334	0.42	0.14	2.375	158.5
Average	1.591	1.686	3.277	1.835	3.277	0.508	0.656	− 0.147	3.456	123.7
Max	3.319	3.087	5.378	3.452	5.378	0.854	1.057	0.85	5.809	188.1
Min	0.706	0.768	1.474	0.853	1.474	0.249	0.306	− 1.37	2.064	67.08
Range	2.613	2.32	3.904	2.599	3.904	0.605	0.751	2.22	3.745	121
σ	0.775	0.74	1.263	0.966	1.263	0.166	0.206	0.656	1.37	35.02
3σ	2.326	2.22	3.788	2.898	3.788	0.498	0.617	1.968	4.11	105.1
Sum	15.91	16.86	32.77	18.35	32.77	5.085	6.555	− 1.474	34.56	1237

Table 11 Surface roughness parameters of PA633GF against SiC of grit size 500

Measurement number	Rp[μm]	Rv[μm]	Rz[μm]	Rc[μm]	Rt[μm]	Ra[μm]	Rq[μm]	Rsk	Rku	Rsm[μm]
1	2.269	1.219	3.487	1.437	3.487	0.567	0.727	0.779	3.064	55.57
2	2.429	1.685	4.114	3.215	4.114	0.815	0.955	0.407	2.194	123.3
3	3.041	2.003	5.045	2.893	5.045	0.667	0.875	0.41	4.446	118.5
4	6.304	5.249	11.55	8.337	11.55	1.785	2.298	− 0.441	3.129	167.2
5	1.744	2.758	4.502	3.358	4.502	0.816	0.985	− 0.349	2.898	132.4
6	1.365	1.155	2.519	1.86	2.519	0.56	0.663	0.307	2.113	118.5
7	1.954	2.534	4.488	3.244	4.488	0.632	0.835	− 0.296	3.77	150.9
8	2.805	2.155	4.96	2.447	4.96	0.862	1.13	− 0.04	2.893	119.9
9	4.129	4.231	8.36	1.729	8.36	1.747	2.107	− 0.375	2.228	216.8
10	3.485	3.006	6.491	2.133	6.491	1.117	1.384	0.15	2.597	125.4
Average	2.952	2.6	5.552	3.065	5.552	0.957	1.196	0.055	2.933	132.8
Max	6.304	5.249	11.55	8.337	11.55	1.785	2.298	0.779	4.446	216.8
Min	1.365	1.155	2.519	1.437	2.519	0.56	0.663	− 0.441	2.113	55.57
Range	4.94	4.094	9.034	6.899	9.034	1.225	1.635	1.22	2.334	161.2
σ	1.44	1.302	2.649	1.975	2.649	0.458	0.57	0.418	0.736	41.16
3σ	4.319	3.906	7.947	5.924	7.947	1.373	1.709	1.254	2.209	123.5
Sum	29.52	26	55.52	30.65	55.52	9.568	11.96	0.551	29.33	1328

increased with the decrease in the grit size number. An improved surface flattening could be seen when the grit size of the counter-face increased from 220 to 1000. The line roughness parameters were softened from ($Ra = 1.416$ μm, $Rz = 16.66$ μm and $Rsm = 212.3$ μm) to ($Ra = 0.508$ μm, $Rz = 3.277$ μm and $Rsm = 123.7$ μm). The line roughness parameters Ra and Rz were smoother for PA6 than PA633GF by 118.9% and 90.9%, respectively, in the abrasion against SiC of the finest grit size. The line roughness parameters for PA650GF against SiC of

Table 12 Surface roughness parameters of PA633GF against SiC of grit size 220

Measurement number	Rp[µm]	Rv[µm]	Rz[µm]	Rc[µm]	Rt[µm]	Ra[µm]	Rq[µm]	Rsk	Rku	Rsm[µm]
1	1.446	1.376	2.823	0.932	2.823	0.373	0.477	0.192	3.277	66.82
2	0.761	0.726	1.487	0.587	1.487	0.264	0.329	− 0.03	2.535	88.18
3	8.001	4.782	12.78	5.637	12.78	2.581	3.058	0.395	2.15	86.36
4	22.87	3.415	26.28	3.356	26.28	1.708	3.535	4.77	28.68	171.3
5	6.998	7.532	14.53	6.31	14.53	1.908	2.534	0.163	3.355	64.02
6	2.423	3.712	6.135	3.195	6.135	1.287	1.487	− 0.503	2.299	263.1
7	14.99	9.343	24.33	8.058	24.33	2.085	2.857	0.83	6.958	121.4
8	3.665	2.018	5.683	2.05	5.683	0.665	0.925	1.114	5.397	70.31
9	19.14	6.307	25.45	14.42	25.45	1.283	2.69	3.818	29.34	494.5
10	44.18	2.898	47.08	47.08	47.08	2.009	6.404	6.374	42.87	697.1
Average	12.45	4.211	16.66	9.162	16.66	1.416	2.43	1.712	12.69	212.3
Max	44.18	9.343	47.08	47.08	47.08	2.581	6.404	6.374	42.87	697.1
Min	0.761	0.726	1.487	0.587	1.487	0.264	0.329	− 0.503	2.15	64.02
Range	43.42	8.617	45.59	46.49	45.59	2.317	6.075	6.877	40.72	633.1
σ	13.55	2.782	14.25	13.94	14.25	0.781	1.797	2.381	15.01	216.5
3σ	40.64	8.347	42.74	41.81	42.74	2.344	5.39	7.144	45.03	649.5
Sum	124.5	42.11	166.6	91.63	166.6	14.16	24.3	17.12	126.9	2123

grit size 1000 were ($Ra = 0.829$ µm, $Rz = 5.481$ µm and $Rsm = 187.9$ µm) and the line roughness parameters for PA650GF against SiC of grit size 220 were ($Ra = 1.819$ µm, $Rz = 19.17$ µm and $Rsm = 348.7$ µm). The addition of the lubricant Molybdenum disulphide was significant in smoothing the surface of the samples after the conclusion of the abrasion process, where the line roughness parameters, Ra, Rz and Rsm for $PA625GF5MoS_2$ were lower than these for PA625GF by 24.8%, 17.9% and 21.4%, respectively. The highest line roughness parameters were obtained for PA650GF samples, which directly relate to their high specific wear rates against all grit sizes.

3.5 Surface Morphology of Worn-Out Surfaces

Figures 12, 13, 14 and 15 show the surface morphologies of the worn-out interfaces at variable magnifications. Figure 12 displays a smooth worn surface with some debris, grooves and cavities, resulting from matrix rubbing and removal. The smooth to mild surface roughness features are attributed to the low contact pressure and the softness of the pure Polyamide material rubbing against the counter-face. In Fig. 13, the lack of support for glass fibres at 25% of fibre volume fraction exposes the matrix to more aggressive micro-ploughing and micro-cutting attacks by the silicon carbide counter-face, which led to a remarkable rise in the specific wear rate. The greater amount of wear debris produced during the abrasion process further reduces the wear resistance of the fibre-rich composite. Overall, no noticeable fibre pull-outs were observed, indicating strong compatibility between the matrices and fibres. The penetration of the matrices through glass fibres demonstrates this strong compatibility. Ripple markings and abrasion grooves were also observed, along with some interface gaps between glass fibres and PA6. The yellow arrows in the figures indicate the direction of abrasion. The debris generated during the abrasive wear action shows that a relatively thick layer of PA6 was peeled off because of the reciprocating shearing state for samples abraded against grit size 500 and grit size 220. Relatively large wear debris is removed from the surfaces. Large grooves and deep irregular cavities are evident in the micrographs in Figs. 14 and 15.

The literature presents conflicting findings on the impact of fibre reinforcement on the wear resistance of polymer composites, with some studies reporting a significant reduction in wear rate and others suggesting a detrimental effect of fibres or solid lubricants. This highlights the idea that the friction and wear behaviour of these materials is not solely governed by their intrinsic properties but instead strongly influenced by the tribological system in which they are employed. Therefore, more comprehensive tribological investigations are needed to fully evaluate the friction and wear performance of polymer composites under different contact conditions.

The surface of glass fibre reinforced PA6 undergoes micro-cracking when exposed to coarse grit size 220. Friction generates heat between counterparts during wear, causing the composite surface to soften and become more susceptible to wear and ploughing. Figures 16, 17 and 18 display the energy-dispersive X-ray spectroscopy
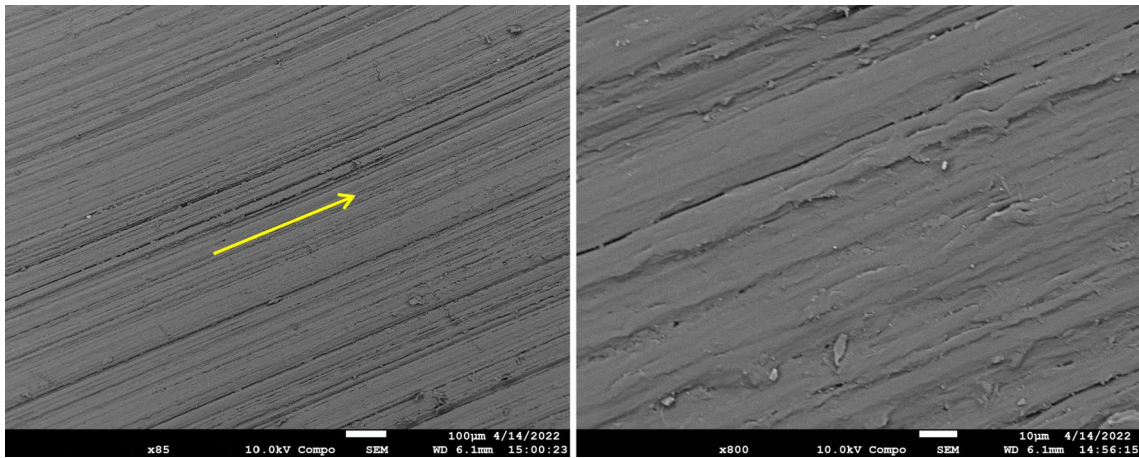
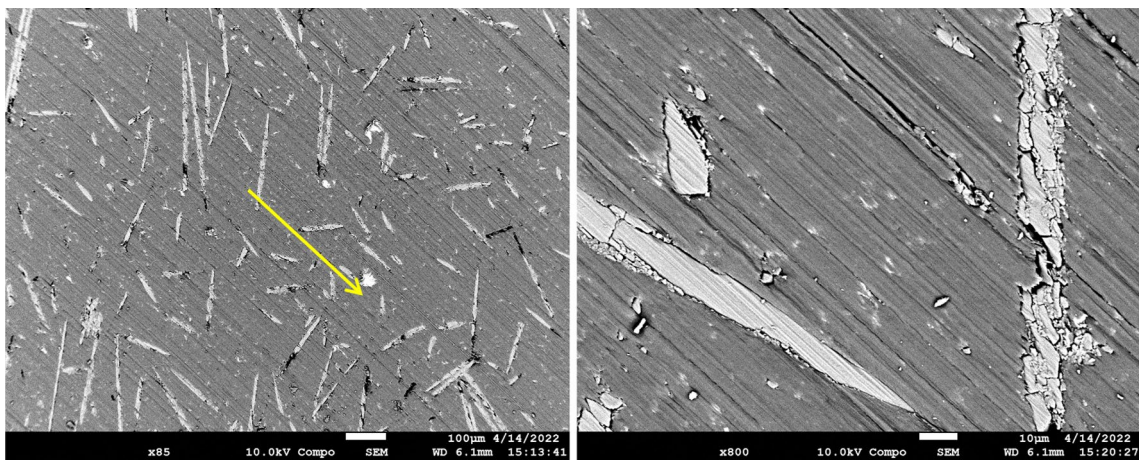**Fig. 12** FESEM images depicting the worn surfaces of PA6 against SiC, grit 1000

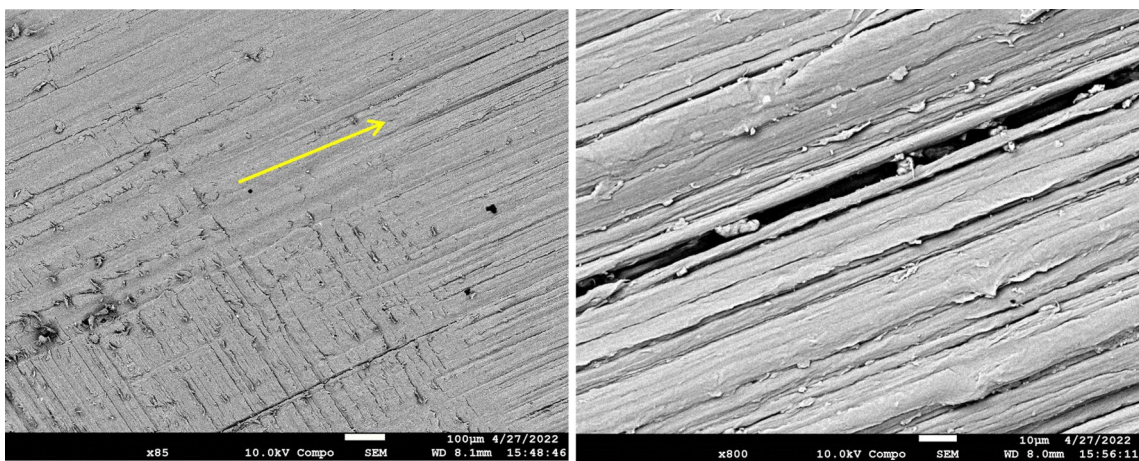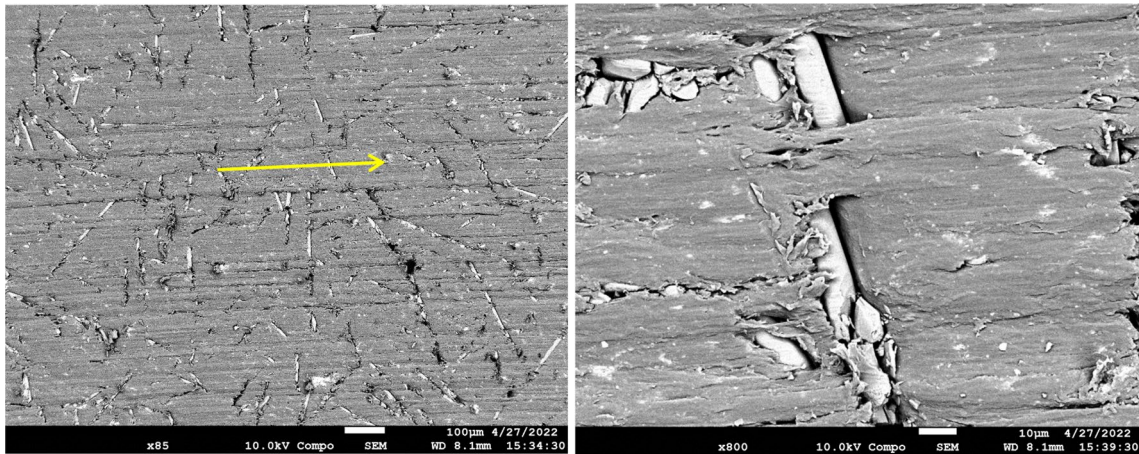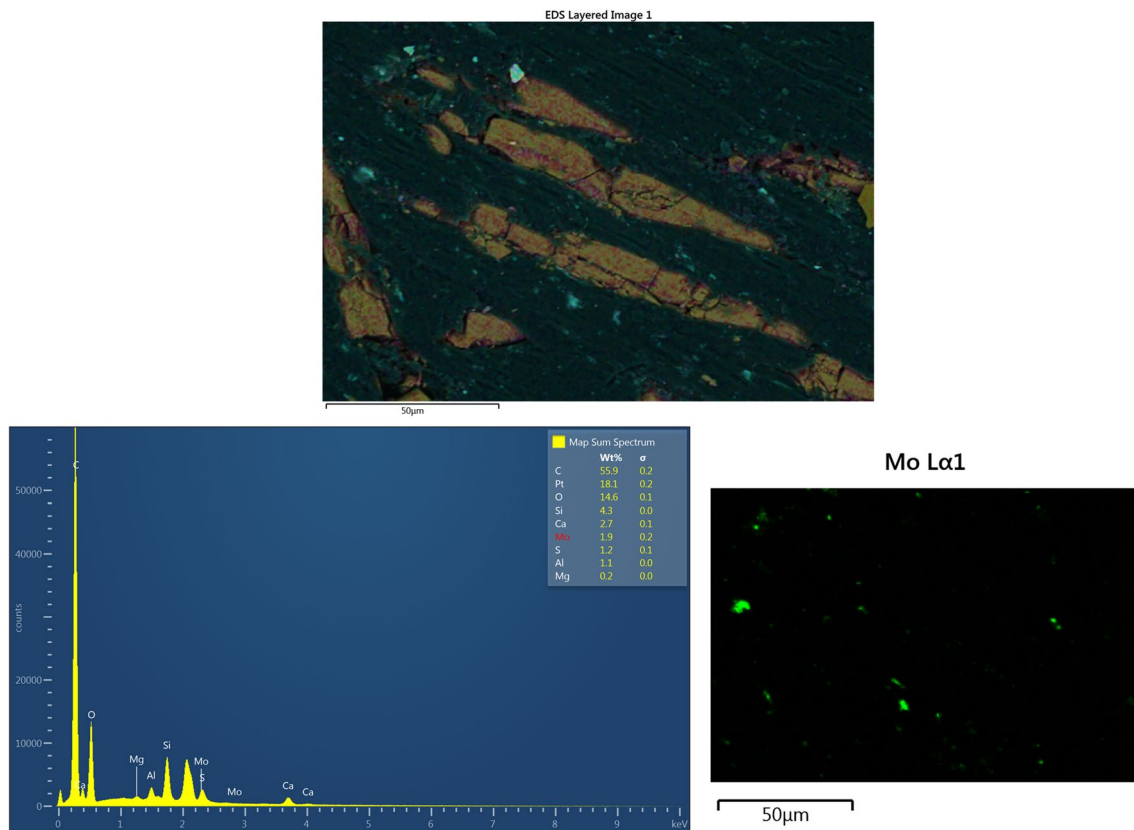**Fig. 13** FESEM images depicting the worn surfaces of PA625GF against SiC, grit 1000

**Fig. 14** FESEM images depicting the worn surfaces of PA6 against SiC, grit 500

Fig. 15 FESEM images depicting the worn surfaces of PA625GF against SiC, grit 500

Fig. 16 Micrograph and EDS elemental analysis of PA625GF containing 5%MoS$_2$, after wearing out against SiC of grit size 1000 and the dot mapping scan of the Molybdenum disulphide lubricant

(EDS) elemental analysis of specimens containing Molybdenum as a lubricant, which is confirmed through mapping images. The presence of obvious and narrow grooves, microcracks, and debris in the figures suggests that the samples suffered the most from abrasive wear when loaded against the coarse grit size. High volume fraction of glass fibres acted as stress concentrators and promoted crack formation. Increasing the reinforcement content may decrease the wear properties of neat polyamide 6. The optimum wear performance was achieved with 33% fibre volume fraction
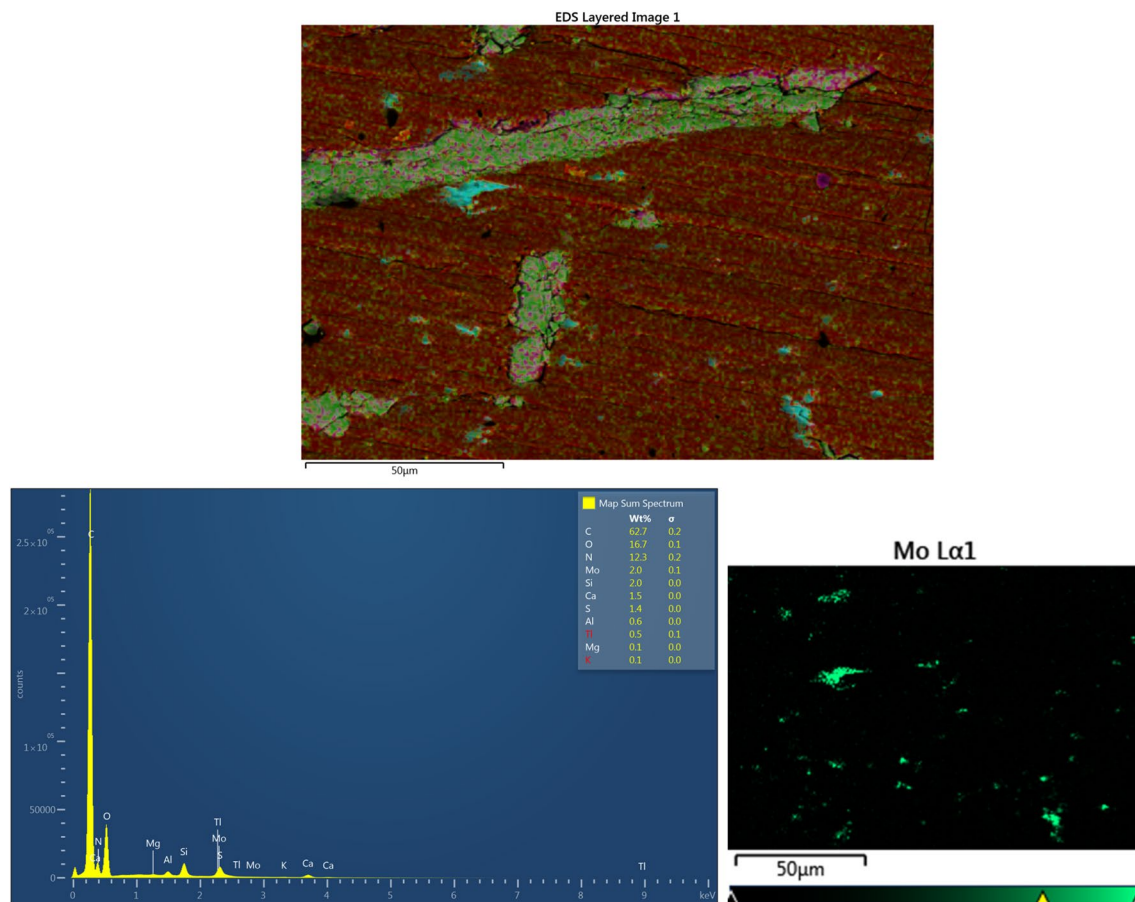
Fig. 17 Micrograph and EDS elemental analysis of PA625GF containing 5%MoS$_2$, after wearing out against SiC of grit size 500 and the dot mapping scan of the Molybdenum disulphide lubricant

of reinforcement, and the addition of lubricant significantly reduced the wear rate of the materials. Figure 19a shows a summary to the abrasive wear of pin samples in a sketch and Fig. 19b displays an overview the engagement between pin samples and abrasive grit papers while the hard SiC abrasive particles are digging into the softer material.

In wear conditions of samples against finer grit sizes, the deterioration of the grits would occur quickly and the removal ability of the material slows down. The fine grit abrasive particles would adversely deteriorate than coarser grit sizes for the applied distance and load [50]. Therefore, it can be deducted that for finer grit sizes, the specific wear rate will be lesser than that for coarser grit sizes. Additionally, the damage of samples become intense when they get abraded against coarse grit size papers owing to the higher penetration depth caused by the coarser abraders. However, the presence of MoS$_2$ presents a self-lubricating layer between the samples and the grinding papers. This layer acts as a sacrificial material and a polishing agent in the abrasion process. This explains the improved wear resistance

for materials containing the filler MoS$_2$ than the unfilled materials.

4 Conclusions and Future Directions

4.1 Conclusions

Tribological properties are some of the most important parameters that influence the material durability and serviceability. In the current work, three different fibre volume fractions of glass fibres were used to reinforce Polyamide 6 by injection moulding and in the presence of MoS$_2$ as a lubricant. The wear mode applied for all materials was the abrasive mode. Three grit sizes of the SiC counter-face were used to assess the grit size influence on the wear performance of materials. Other mechanical properties were evaluated including compressing testing and tensile testing. Surface roughness parameters on worn-out samples were executed by optical microscopy. The morphological analysis and elemental analysis were carried out on worn-out
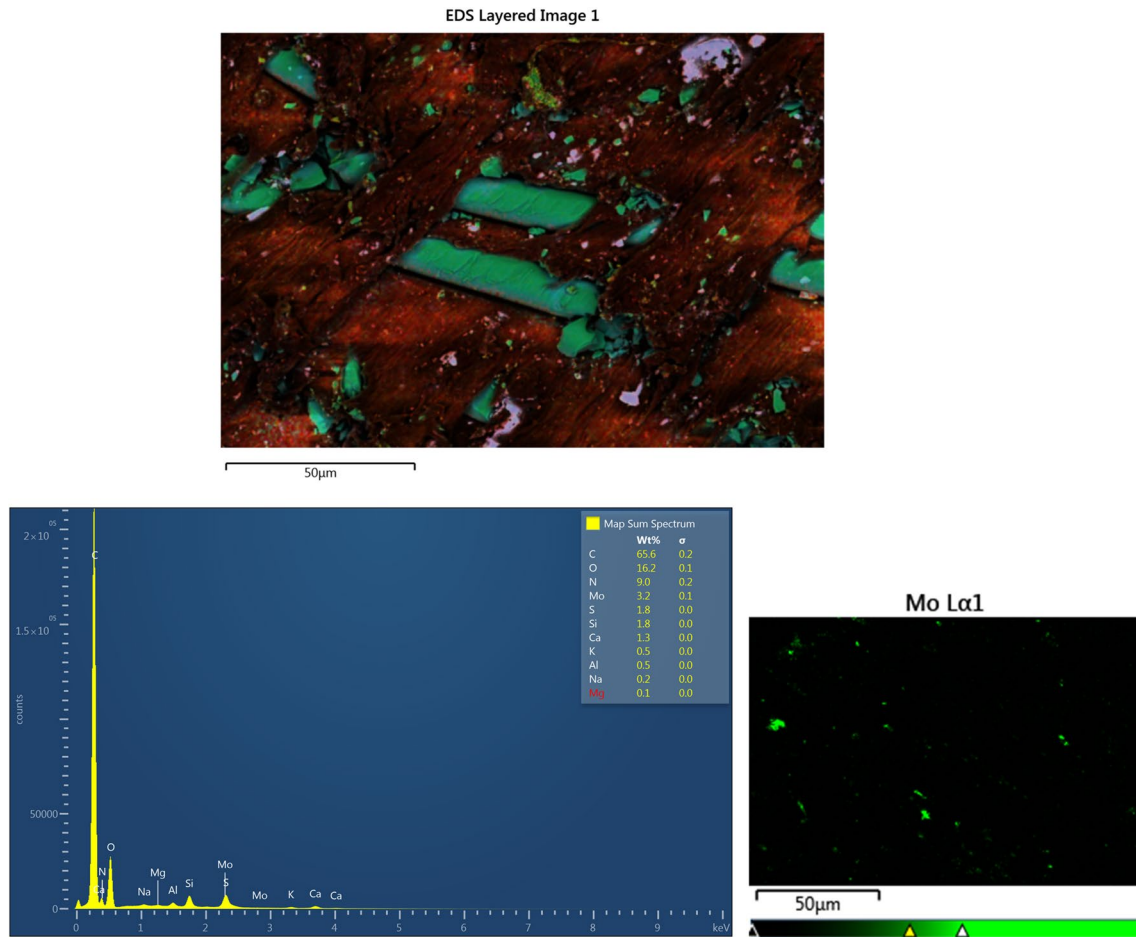
Fig. 18 Micrograph and EDS elemental analysis of PA625GF containing 5%MoS$_2$, after wearing out against SiC of grit size 220 and dot mapping scan of the Molybdenum disulphide lubricant

Fig. 19 **a** A schematic illustration of the abrasion process; and **b** Pin to Counter-face engagement and close view of abrasive grits digging into the material
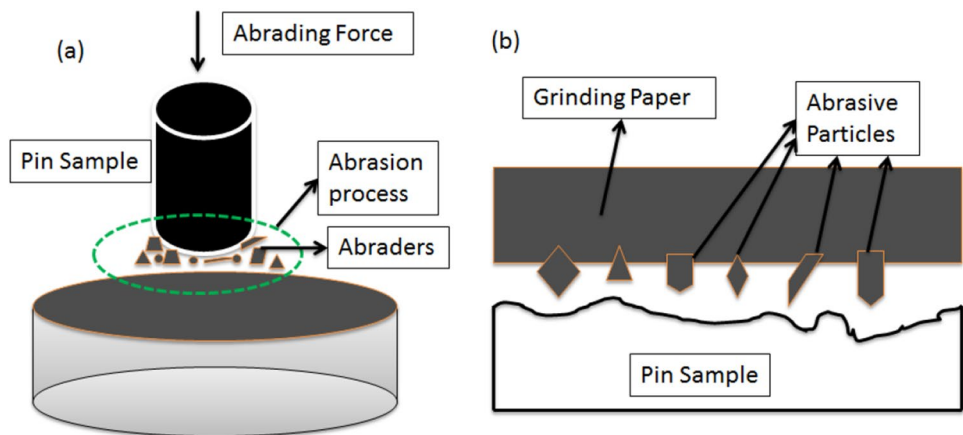
surfaces. The following summary is a set observation concluded from this study:

- The increase in fibre volume fraction from 33 to 50% was detrimental to the specific wear rate of materials, where

the addition of 50% of glass fibres led to an increase in specific wear rate by 167% than pure PA6.

- The incorporation of the lubricant MoS$_2$ showed a significant enhancement in the wear resistance of the materials against all grit sizes, whereas the average improvement

in specific wear rate was 18.84%. The wear tracks of PA6 composite samples exhibited smoother wear surfaces, which indicate that the materials were protected from further deterioration due to the presence of molybdenum disulphide.

- The optimum fibre volume fraction that showed the least specific wear rate among the other fractions, was 33%, with the specific wear rate of PA633GF being less than these of PA625GF and PA650GF by 30.59% and 44.07%, respectively.
- The increase in the grit size of the SiC counter-face material was inversely proportional to the specific wear rate of PA6 and PA6 composite variations. At low grit size, the penetration depth was higher which causes damage to the materials. This indicates that the wear of PA6 and glass fibre reinforced PA6 can be severe under highly abrasive conditions.
- The surface roughness parameters of worn-out surfaces were directly proportional to the wear amount, such that smooth surfaces corresponded to less wear volume and rough surfaces corresponded to high wear volume.

4.2 Future Directions of Wear and Friction

The future direction of tribology remains challenging to ascertain due to the inherent uncertainties associated with extrapolating from the present to the future. However, the subsequent essential research requirements are identified with utmost priority for the upcoming research directions:

- Crucial considerations to be considered during the advancement of tribo-materials pertain to their sustainability and the broader economic implications. Thorough tribological inquiries are imperative to elucidate strategies for enhancing the longevity of tribo-materials, mitigating environmental effects through the implementation of biodegradable lubricants and greases, as well as establishing effective recycling methodologies for tribo-materials.
- Evaluating abrasion resistance through the application of diverse methodologies and tools, such as the use of micro-CT to evaluate and predict the wear amount of materials. Additionally, efforts can be made to establish a correlation between tribological properties and dynamic attributes of materials including impact strength, compressive strength and surface roughness.
- Advancement of surface coating technologies can be pursued for enhancing the wear resistance of tribo-elements.
- Creation of wear and failure maps as valuable tools in machine tribo-element design.

- Thorough investigations are required to ascertain the influence of vibrations on the behaviour of tribo-systems.
- The utilization of artificial neural networks in wear analysis presents an opportunity to discern the optimal coating materials for diverse substrates, effectively augmenting their wear resistance through precise predictions. This approach proves more efficient and less time-consuming compared to conventional methods for identifying such coating materials.

Declarations

Conflict of interest The authors have no financial or proprietary interests in any material discussed in this article.

References

1. Zaghloul, M.M.Y., et al.: Wear behaviour of polymeric materials reinforced with man-made fibres: a comprehensive review about fibre volume fraction influence on wear performance. J. Reinf. Plast. Compos. **41**(5–6), 215–241 (2021). https://doi.org/10.1177/07316844211051733

2. Zaghloul, M.M.Y.: Effect of Nano Particles on the Mechanical Properties of Thermosetting Polymeric Materials Reinforced with Glass Fibers, MSc Thesis. Faculty of Engineering, Alexandria University (2018)

3. Zaghloul, M., Mahmoud, Y., et al.: Developments in polyester composite materials—An in-depth review on natural fibres and nano fillers. Compos. Struct. **278**, 114698 (2021)

4. Zaghloul, M.M.Y., Steel, K., Veidt, M., Heitzmann, M.T.: Mechanical and tribological performances of thermoplastic polymers reinforced with glass fibres at variable fibre volume fractions. Polymers **15**, 694 (2023). https://doi.org/10.3390/polym15030694

5. Cao, S., et al.: Microstructure evolution and wear resistance of in-situ nanoparticles reinforcing Fe-based amorphous composite coatings. Surf. Interfaces **21**, 100652 (2020). https://doi.org/10.1016/j.surfin.2020.100652

6. Zaghloul, M.Y., Zaghloul, M.M.Y., Zaghloul, M.M.Y.: Influence of stress level and fibre volume fraction on fatigue performance of glass fibre-reinforced polyester composites. Polymers **14**(13), 2662 (2022). https://doi.org/10.3390/polym14132662

7. Fuseini, M., Zaghloul, M.M.Y., Elkady, M.F., et al.: Evaluation of synthesized polyaniline nanofibres as corrosion protection film coating on copper substrate by electrophoretic deposition. J. Mater. Sci. **57**(10), 6085–6101 (2022). https://doi.org/10.1007/s10853-022-06994-3

8. Zaghloul, M.M.Y., Mohamed, Y.S., El-Gamal, H.: Fatigue and tensile behaviors of fiber-reinforced thermosetting composites embedded with nanoparticles. J. Compos. Mater. **53**(6), 709–718 (2018). https://doi.org/10.1177/0021998318790093

9. Fuseini, M., Zaghloul, M.M.Y.: Statistical and qualitative analyses of the kinetic models using electrophoretic deposition of polyaniline. J. Ind. Eng. Chem. **113**, 475–487 (2022). https://doi.org/10.1016/j.jiec.2022.06.023

10. Zaghloul, M.M.Y.M.: Mechanical properties of linear low-density polyethylene fire-retarded with melamine polyphosphate. J. Appl. Polym. Sci. **135**(46), 46770 (2018). https://doi.org/10.1002/app.46770

11. Fuseini, M., Zaghloul, M.M.Y.: Investigation of electrophoretic deposition of PANI nano fibers as a manufacturing technology for corrosion protection. Prog. Org. Coat. **171**, 107015 (2022). https://doi.org/10.1016/j.porgcoat.2022.107015

12. Zaghloul, M.M.Y., Zaghloul, M.M.Y., Fuseini, M.: Recent progress in Epoxy Nanocomposites: corrosion, structural, flame retardancy and applications — A comprehensive review. Polym Adv Technol. (2023). https://doi.org/10.1002/pat.6144

13. Mahmoud Zaghloul, M.Y., Yousry Zaghloul, M.M., Yousry Zaghloul, M.M.: Physical analysis and statistical investigation of tensile and fatigue behaviors of glass fiber-reinforced polyester via novel fibers arrangement. J. Compos. Mater. **57**(1), 147–166 (2023). https://doi.org/10.1177/00219983221141154

14. Zaghloul, M.M.Y., Zaghloul, M.Y.M., Zaghloul, M.M.Y.: Experimental and modeling analysis of mechanical-electrical behaviors of polypropylene composites filled with graphite and MWCNT fillers. Polym. Test **63**, 467–474 (2017). https://doi.org/10.1016/j.polymertesting.2017.09.009

15. Zaghloul, M.M.Y., Zaghloul, M.M.Y.: Influence of flame retardant magnesium hydroxide on the mechanical properties of high density polyethylene composites. J. Reinf. Plast. Compos. **36**(24), 1802–1816 (2017). https://doi.org/10.1177/0731684417727143

16. Mohamed, Y.S., El-Gamal, H., Zaghloul, M.M.Y.: Micro-hardness behavior of fiber reinforced thermosetting composites embedded with cellulose nanocrystals. Alexandria Eng. J. **57**(4), 4113–4119 (2018). https://doi.org/10.1016/j.aej.2018.10.012

17. Rashid, B., Leman, Z., Jawaid, M., et al.: Dry sliding wear behavior of untreated and treated sugar palm fiber filled phenolic composites using factorial technique. Wear **380–381**, 26–35 (2017)

18. Omrani, E., Menezes, P.L., Rohatgi, P.K.: State of the art on tribological behavior of polymer matrix composites reinforced with natural fibers in the green materials world. Eng. Sci. Technol. Int. J. **19**, 717–736 (2016)

19. Mohazzab, B.F., et al.: Laser Surface treatment of pure titanium: microstructural analysis, wear properties, and corrosion behavior of titanium carbide coatings in hank's physiological solution. Surf.

20. Dasari, A., Yu, Z.-Z., Mai, Y.-W., et al.: Clay exfoliation and organic modification on wear of nylon 6 nanocomposites processed by different routes. Compos. Sci. Technol. **65**, 2314–2328 (2005)

21. Mao, K., Greenwood, D., Ramakrishnan, R., Goodship, V., Shrouti, C., Chetwynd, D., Langlois, P.: The wear resistance improvement of fibre reinforced polymer composite gears. Wear **426–427**, 1033–1039 (2019)

22. Morioka, Y., Tsuchiya, Y., Shioya, M.: Correlations between the abrasive wear, fatigue, and tensile properties of filler-dispersed polyamide 6. Wear **338–339**, 297–306 (2015)

23. Kumar, S., Panneerselvam, K.: Two-body abrasive wear behavior of nylon 6 and glass fiber reinforced (GFR) nylon 6 composite. Proc. Technol. **25**, 1129–1136 (2016)

24. Suresha, B., Chandramohan, G., Siddaramaiah, H., et al.: Three-body abrasive wear behaviour of carbon and glass fiber reinforced epoxy composites. Mater. Sci. Eng. A **443**, 285–291 (2007)

25. Tong, J., Ma, Y., Arnell, R.D., et al.: Free abrasive wear behavior of UHMWPE composites filled with wollastonite fibers. Compos. Part A **37**, 38–45 (2006)

26. Khan, A., Ahmad, M.A., Joshi, S., et al.: Abrasive wear behavior of chemically treated coir fibre filled epoxy polymer composites. Am. J. Mech. Eng. Autom. **1**, 1–5 (2014)

27. Venkategowda, T., et al.: Adhesive and abrasive wear behavior of Kenaf long fiber reinforced epoxy composites. Mater. Today **45**, 150–155 (2021)

28. Anand Chairman, C., et al.: Abrasive wear characteristics of bio-based jatropha oil cake incorporated basalt fiber reinforced epoxy composites. Mater. Today **33**, 3947–3950 (2020)

29. Kumar, S., et al.: Experimental investigation of three-body abrasive wear behavior of rice husk filled polylactic acid (PLA) composites. Mater. Today **52**, 599–603 (2022)

30. Lee, H.G., et al.: Effect of compacted wear debris on the tribological behavior of carbon/epoxy composites. Compos. Struct. **74**(2), 136–144 (2006). https://doi.org/10.1016/j.compstruct.2005.03.014

31. Second, S.: The influence of carbon fiber content on the tribological properties of PA6 composites. J. Reinf. Plast. Compos. **29**, 771–778 (2010). https://doi.org/10.1177/0731684408100695

32. Zhou, S., Zhang, Q., Wu, C., Huang, J.: Effect of carbon fibre reinforcement on the mechanical and tribological properties of polyamide6/polyphenylene sulfide composites. Mater. Des. **44**, 493–499 (2013). https://doi.org/10.1016/j.matdes.2012.08.029

33. Jayachamarajendra, S.: Three-body abrasive wear behaviour of polyurethane composites. J. Compos. Mater. **41**, 2701–2713 (2007). https://doi.org/10.1177/0021998307078730

34. Mohanty, J.R., Das, S.N., Das, H.C.: Effect of fiber content on abrasive wear behavior of date palm leaf reinforced polyvinyl pyrrolidone composite. Int. Sch. Res. Not. **2014**, 10 (2014). https://doi.org/10.1155/2014/453924

35. Li M, Luo R.: (2015) Effect of carbon fibre content on mechanical and tribological properties of carbon/phenolic resin composites. In 5th International Conference on Information Engineering for Mechanics and Materials (ICIMM 2015). pp. 539–42

36. Zhang, X., Li, K., Li, H., Fu, Y., Fei, J.: Tribological and mechanical properties of glass fiber reinforced paper-based composite friction material. Tribol. Int. **69**, 156–167 (2014). https://doi.org/10.1016/j.triboint.2013.08.003

37. Ma, N., Lin, G.M., Xie, G.Y., Sui, G.X., Yang, R.: Tribological behavior of polyetheretherketone composites containing short carbon fibers and potassium titanate whiskers in dry sliding against steel. J. Appl. Polym. Sci. **123**, 740–748 (2012). https://doi.org/10.1002/app.34502

38. Shard, A., Chand, R., Nauriyal, S., et al.: Fabrication and analysis of wear properties of polyetherimide composite reinforced with carbon fiber. J. Fail. Anal. Preven. **20**, 1388–1398 (2020). https://doi.org/10.1007/s11668-020-00943-5

39. Haiter Lenin, A., et al.: A statistical prediction on wear and friction behavior of ZrC nano particles reinforced with Al Si composites using full factorial design. Surf. Interfaces **10**, 149–161 (2018). https://doi.org/10.1016/j.surfin.2018.01.003

40. Yongxin, P., et al.: Wear properties of polyetherimide and carbon fiber-reinforced polyetherimide composite. J. Thermoplast. Compos. Mater. **27**(7), 949–957 (2014). https://doi.org/10.1177/0892705712461514

41. ASTM D638-10. Standard test method for 'Tensile properties of polymer matrix composite materials'. West Conshohocken, PA: American Society for Testing and Materials (ASTM) International, 2000.

42. ASTM D695-15. Standard Test Method for Compressive Properties of Rigid Plastics, ASTM International, West Conshohocken, PA, USA, 2015. 10.1520/D 069 5-15

43. ASTM D792-00. (2000) Standard test method for 'Density and Specific Gravity (Relative Density) of Plastics by Displacement'. American Society for Testing and Materials (ASTM) International, West Conshohocken.

44. ASTM G99-17 (2017) Standard test method for 'Wear Testing with a Pin-on-Disk Apparatus'. American Society for Testing and Materials (ASTM) International, West Conshohocken

45. Palabiyik, M., Bahadur, S.: Tribological studies of polyamide 6 and high-density polyethylene blends filled with PTFE and copper oxide and reinforced with short glass fibers. Wear **253**(3–4), 369–376 (2002). https://doi.org/10.1016/s0043-1648(02)00144-8

46. Stachowiak, G.W., Batchelor, A.W.: Engineering tribology, 3rd edn., p. 619. Elsevier Science, Amsterdam (2005)

47. Ratner, S.B., Farberova, I.I., Radyukevich, O.V., et al.: Connection between wear resistance of plastics and other mechanical properties. Soviet Plastic **7**, 37–45 (1964)

48. Kim, J.I., Kim, J.W., Ryu, S.H.: Wear characteristics of exfoliated MoS2/polyamide-6,6 composite. J. Elastomers Plast. **54**(2), 374–384 (2022). https://doi.org/10.1177/00952443211047072

49. Neis, P.D., Ferreira, N.F., Poletto, J.C., Sukumaran, J., Andó, M., Zhang, Y.: Tribological behavior of polyamide-6 plastics and their potential use in industrial applications. Wear **376–377**, 1391–1398 (2017). https://doi.org/10.1016/j.wear.2017.01.090

50. Hu, K.H., Hu, X.G., Wang, J., et al.: Tribological properties of MoS2 with different morphologies in high-density polyethylene. Tribol. Lett. **47**, 79–90 (2012)

51. Ch KN, Rao R N.: Effect of Load and Grit Size on High Stress Abrasive Wear of Al-Mg-Si Hybrid Composites. TMS 2016: 145thAnnual Meeting & Exhibition: Supplemental Proceedings, pp. 119–125. (2016). https://doi.org/10.1002/9781119274896.ch15

52. Odabas, D.: Effects of load and speed on wear rate of abrasive wear for 2014 Al alloy. IOP Conf. Ser. **295**, 012008 (2018). https://doi.org/10.1088/1757-899x/295/1/012008

53. Hakami, F., Pramanik, A., Basak, A., Ridgway, N., Islam, M.: Effect of abrasive particle size on tribological behavior of elastomers. Proc. Inst. Mech. Eng. Part J **234**(3), 373–385 (2020). https://doi.org/10.1177/1350650119864486

54. Johnson, R.W.: A study of the pickup of abrasive particles during abrasion of annealed aluminium on silicon carbide abrasive. Wear **16**, 351–358 (1970)